AD-A074 260 MARTIN MARIETTA LABS BALTIMORE MD F/G 20/4
SEPARATION JUMP AND SUDDEN STALL OVER AN ELLIPSOIDAL WING AT IN--ETC(U)
MAY 79 K C WANG F49620-76-C-0004
UNCLASSIFIED MML-TR-79-22C AFOSR-TR-79-0965 NL

| OF |
AD A074260

END
DATE FILMED
10-79
DDC

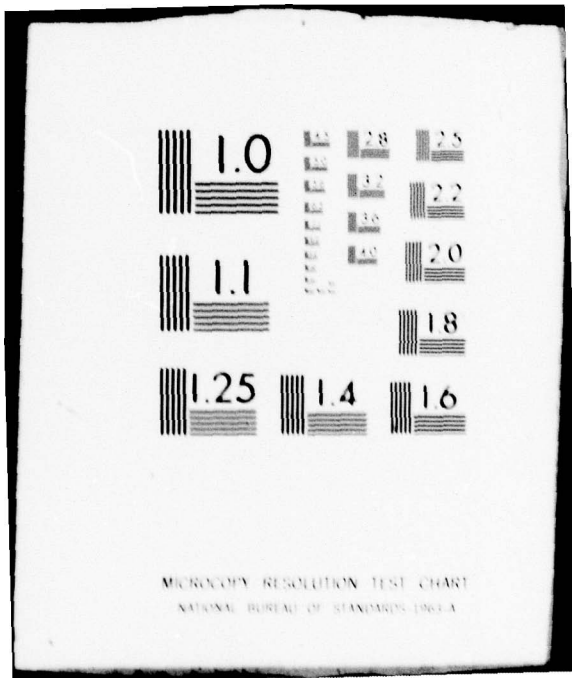
1.0
1.1
1.25
1.4
1.6
2.8
2.5
2.2
2.0
1.8
MICROCOPY RESOLUTION TEST CHART
NATIONAL BUREAU OF STANDARDS 1963-A

MARTIN MARIETTA

(7)

LEVEL II

MML TR 79-22c

SEPARATION JUMP AND SUDDEN STALL OVER AN ELLIPSOIDAL WING AT INCIDENCE

K. C. Wang

May 1979

Research sponsored by the Air Force Office of Scientific Research (AFSC), United States Air Force under Contract F49620-76-C-0004

SEPARATION JUMP AND SUDDEN STALL OVER AN ELLIPSOIDAL WING AT INCIDENCE

K. C. Wang

MML TR 79-22c

May 1979

Research Sponsored by the Air Force Office of Scientific Research (AFSC), United States Air Force, under Contract F49620-76-C-0004

Martin Marietta Corporation
Martin Marietta Laboratories
1450 South Rolling Road
Baltimore, Maryland 21227

Unclassified

SECURITY CLASSIFICATION OF THIS PAGE (When Data Entered)

REPORT DOCUMENTATION PAGE	READ INSTRUCTIONS BEFORE COMPLETING FORM
1. REPORT NUMBER: AFOSR-TR-79-0965	2. GOVT ACCESSION NO. / 3. RECIPIENT'S CATALOG NUMBER
4. TITLE (and Subtitle): Separation Jump and Sudden Stall Over an Ellipsoidal Wing at Incidence .	5. TYPE OF REPORT & PERIOD COVERED: Technical Report.
	6. PERFORMING ORG. REPORT NUMBER: MML-TR-79-22c
7. AUTHOR(s): K. C. Wang	8. CONTRACT OR GRANT NUMBER(s): F49620-76-C-0004
9. PERFORMING ORGANIZATION NAME AND ADDRESS: Martin Marietta Laboratories, Martin Marietta Corporation, 1450 S. Rolling Road, Balto., MD 21227	10. PROGRAM ELEMENT, PROJECT, TASK AREA & WORK UNIT NUMBERS
11. CONTROLLING OFFICE NAME AND ADDRESS: Air Force Office of Scientific Research, Building 410, Bolling AFB, Wash., D. C. 20332	12. REPORT DATE: May 1979 / 13. NUMBER OF PAGES: 42
14. MONITORING AGENCY NAME & ADDRESS (if different from Controlling Office): 51p.	15. SECURITY CLASS. (of this report): Unclassified / 15a. DECLASSIFICATION/DOWNGRADING SCHEDULE

16. DISTRIBUTION STATEMENT (of this Report)

Approved for public release; distribution unlimited.

2304 A3

17. DISTRIBUTION STATEMENT (of the abstract entered in Block 20, if different from Report)

18. SUPPLEMENTARY NOTES

19. KEY WORDS (Continue on reverse side if necessary and identify by block number)

Numerical solutions; Wing theory; 3-D boundary layer; Flow separation; Aerodynamic stall.

20. ABSTRACT (Continue on reverse side if necessary and identify by block number)

To obtain complete and rigorous solutions of the three-dimensional, laminar boundary layer over a finite airplane wing, a flat ellipsoid was chosen as a model to generate concrete results. Initial efforts were directed toward calculating the inviscid flow and the selection of coordinate system, and this was followed by a detailed investigation of the boundary layer restricted to the symmetry-plane. This investigation showed that as the incidence increases, the separation point on the upper surface does not always move continuously forward; instead, it first moves forward and later rearward.

DD FORM 1 JAN 73 1473 407 998

(Contd. reverse side)

SECURITY CLASSIFICATION OF THIS PAGE (When Data Entered)

Then, at a critical incidence, it jumps forward and moves thereafter close to the leading edge. This "separation jump" phenomenon was further found to be little affected by varying the span, but critically dependent on the chord: a longer chord prompts a larger jump. Although such separation jump has been reported for a body of revolution, it has not yet been reported for wing surfaces. The significance of this phenomenon is apparent when one considers that the separation jump may well occur on airplane wings in general and probably accounts for what we might call "sudden stall."

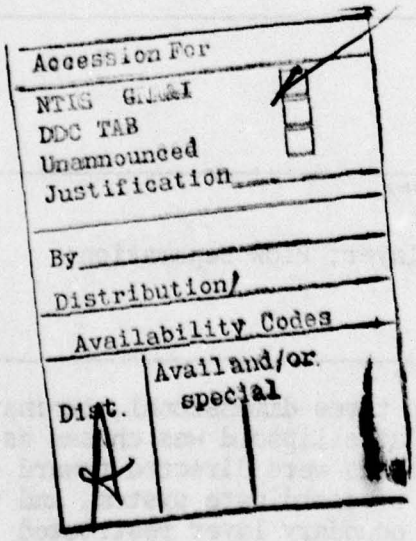

CONTENTS

		Page
SUMMARY		
1.	INTRODUCTION	1
2.	THE COORDINATE SYSTEMS	5
	2.1 Ellipsoidal Coordinates	5
	2.2 Ellipsoidal Transformation	7
	2.3 Boundary Layer Coordinates	10
3.	INVISCID FLOW INPUTS	12
	3.1 Velocity Potential	12
	3.2 Surface Flow in Terms of (μ,θ)	13
	3.3 Pressure Distribution	17
4.	SYMMETRY-PLANE BOUNDARY LAYER	18
	4.1 Boundary Layer Equations	19
	4.2 Method of Solution	21
	4.3 Results	22
	4.3.1 Case 1 - Typical Planform	22
	4.3.2 Case 2 - Shorter Span	28
	4.3.3 Case 3 - Longer Chord	28
	4.3.4 Case 4 - Shorter Chord	31
	4.3.5 Separation vs Incidence	31
	4.3.6 Jump Mechanism	34
	4.3.7 Sudden Stall	34
5.	CONCLUSIONS	37
6.	REFERENCES	39
APPENDIX - EVALUATION OF INTEGRALS		41

SUMMARY

To obtain complete and rigorous solutions of the three-dimensional, laminar boundary layer over a finite airplane wing, a flat ellipsoid was chosen as a model to generate concrete results. Initial efforts were directed toward calculating the inviscid flow and the selection of coordinate system, and this was followed by a detailed investigation of the boundary layer restricted to the symmetry-plane. This investigation showed that as the incidence increases, the separation point on the upper surface does not always move continuously forward; instead, it first moves forward and later rearward. Then, at a critical incidence, it jumps forward and moves thereafter close to the leading edge. This "separation jump" phenomenon was further found to be little affected by varying the span, but critically dependent on the chord: a longer chord prompts a larger jump. Although such separation jump has been reported for a body of revolution, it has not yet been reported for wing surfaces. The significance of this phenomenon is apparent when one considers that the separation jump may well occur on airplane wings in general and probably accounts for what we might call "sudden stall."

1. INTRODUCTION

For aerospace applications, two typical body geometries are of particular importance for fluid dynamics study: an elongated body such as a fuselage or missile, and a flat wing. While our recent three-dimensional boundary layer research has been largely restricted to the body problem[1,2], the present study focused on the wing.

Investigation of the wing's boundary layer has been for the most part restricted to an infinite yawed wing[3,4,5], for which the method and concept are essentially two-dimensional. A complete and rigorous solution for the boundary layer over a finite wing has been hampered by at least two factors. First, until recent years, calculation for a three-dimensional boundary problem was impractical. Second, the corresponding inviscid solutions have been inadequate. Classical linearized lifting-wing theory yields a singular solution at the edges which, in turn, prevents the boundary layer there from being determined. The result is not only that the boundary layers on the upper and lower surfaces must be treated separately, as if they were independent, but also that flow separation cannot be accurately determined. (Accurate calculations of the leading-edge boundary layer are critical to accurate determination of flow separation, as will be seen later.) On the experimental side, three-dimensional boundary layer investigation has been largely limited to surface-flow visualization, and quantitative measurement has been rare and fragmentary.

In this study, we choose a flat ellipsoid as a wing model. Fig. 1 shows the flow diagram where a, b and c denote the semi-axes along the

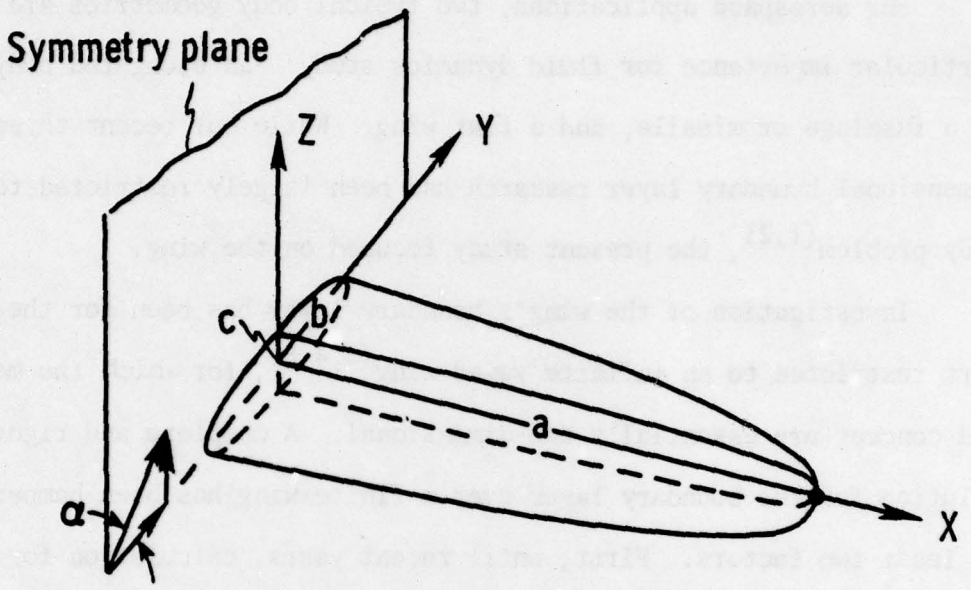

Fig. 1. Ellipsoidal Wing

X, Y, Z-direction. Since the exact inviscid solution[6] for an ellipsoid is known in simple closed form, our efforts to obtain concrete solutions were considerably simplified. This model allowed us to study thoroughly various basic aspects of the boundary layer over a wing-like geometry. A flat ellipsoid does not embrace all of the lifting characteristics of a real, finite wing. However, rigorous treatment of a real wing would necessarily require the hookup of two extensive computing programs, one for the inviscid calculation and one for the three-dimensional boundary layer calculation. The task is straightforward, but time-consuming. In addition, numerical solutions do not usually yield accurate pressure gradients or

even higher derivatives without special efforts. Such elaborate calculations are perhaps better suited to future refinements. In the early 1950's, Zaat, et al.[8] attempted to calculate the boundary layer on a flat ellipsoid; however, this calculation was restricted to the flat portion of the body and only scanty results were reported.

The present study was concerned with the symmetry-plane boundary layer over an ellipsoidal wing. As restricted as this problem may be, similar investigations previously for an inclined body of revolution[9,10] revealed new features of fundamental significance. Among them was the "separation jump" phenomenon, referring to the sudden movement of the separation point on the leeside symmetry-plane as the incidence continues to increase. As the incidence increases from zero, the separation point moves only slowly, remaining near the rear end of the inclined body; but upon reaching a critical incidence, the separation point "jumps" to the front end. In the case of a spheroid of thickness ratio 1/4, this critical incidence was found to be around 40°. It was also found[11,12] that accompanying such discontinuous change of the separation point on the leeside symmetry-plane, there is a corresponding change of the separation pattern on the whole body from an open-type of separation to a closed-type of separation. This observation has changed the conception of three-dimensional flow separation. More recently, Cebeci, Khattab and Stewartson[13] further concluded through an asymptotic formulation that the same critical incidence holds also for thinner spheroid even in the limit of zero thickness.

The present study has found a similar separation jump phenomenon. This was unexpected partly because of the wide differences between a body flow and a wing flow, and partly because no such separation jump was ever

reported for a wing-like obstacle in the literature. Why this phenomenon has eluded the attention of researchers thus far is puzzling. It may be due to the fact that detailed boundary layer calculations were not systematically carried out to a sufficiently high incidence. The same is true for the body of revolution problem prior to our previous publications[9,10]. Although it has long been known that when a short separation bubble on an airfoil bursts into a long one, there results a sudden change of separation point; the idea of separation jump considered here is a distinct phenomenon.

To establish some basic trends, calculations were repeated for the ellipsoid with different axis-ratios. This report for the most part presents these findings (section 4) following discussions on the coordinate systems in section 2 and the inviscid solutions in section 3.

2. COORDINATE SYSTEMS

Several coordinate systems were referred to in the present wing problem. To avoid confusion, a brief discussion of them follows in order to make clear why they are introduced and how they are related to one another.

2.1 Ellipsoid Coordinates

The introduction of an ellipsoidal coordinate system[6] is for the purpose of obtaining the incompressible, potential flow solution by the classical method of separation of variables. We begin with the basic ellipsoid in terms of the rectangular coordinates (Fig. 1),

$$\frac{X^2}{a^2} + \frac{Y^2}{b^2} + \frac{Z^2}{c^2} = 1, \qquad a^2 > b^2 > c^2, \tag{1}$$

then form,

$$\frac{X^2}{a^2+\lambda} + \frac{Y^2}{b^2+\lambda} + \frac{Z^2}{c^2+\lambda} = 1. \tag{2}$$

Corresponding to values of λ from $-a^2$ to ∞, the result is a large family of confocal quadric surfaces. The values of λ may be divided into three groups denoted by (ξ, η, ζ) in accordance with

$$-a^2 \leq \zeta \leq -b^2 \leq \eta \leq -c^2 \leq \xi < \infty.$$

Then the surface ξ = constant represents a family of ellipsoids with $\xi = 0$ being the basic ellipsoid, η = constant a family of hyperboloid of

of one sheet and ζ = constant a family of hyperboloid of two sheets. The intersecting curves between these three families of surfaces define a set of ellipsoidal coordinates. Fig. 2a shows a set of three such coordinate surfaces, while Figs. 2b and c present top views of the coordinate lines on the basic ellipsoid.

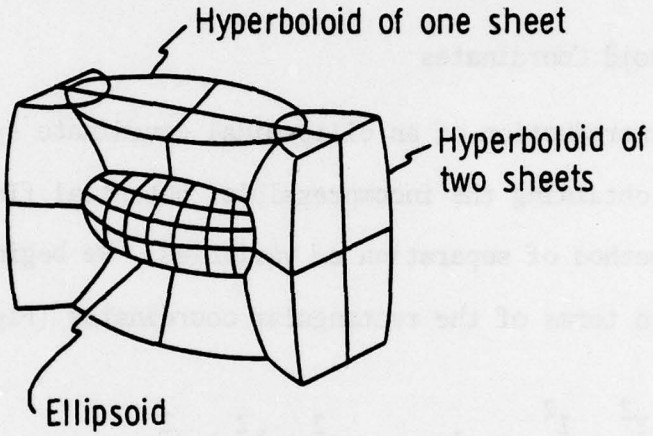

(a) Coordinate surfaces (from Ref. 7)

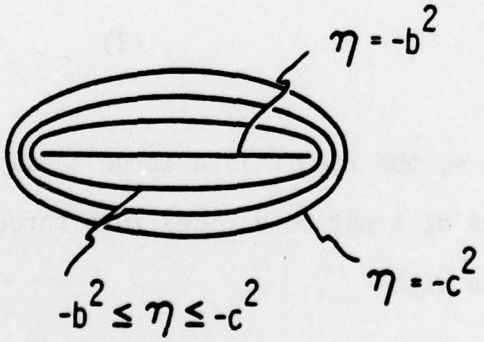

(b) η-constant lines

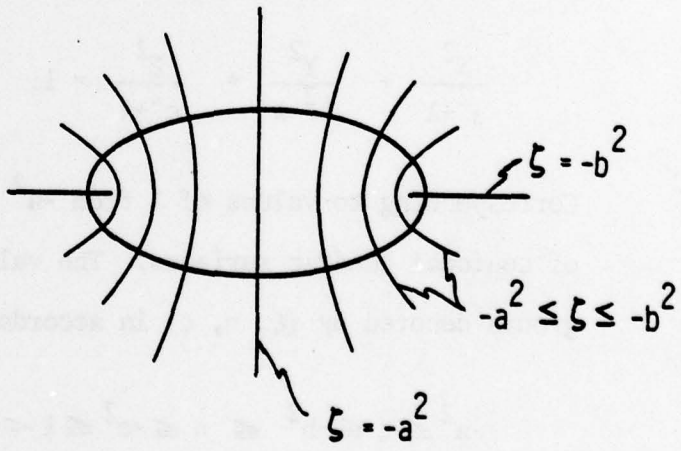

(c) ζ-constant lines

Fig. 2. Ellipsoidal coordinates

The relations between (ξ, η, ζ) and (X, Y, Z) are

$$X^2 = \frac{(a^2+\xi)(a^2+\eta)(a^2+\zeta)}{(a^2-b^2)(a^2-c^2)},$$

$$Y^2 = \frac{(b^2+\xi)(b^2+\eta)(b^2+\zeta)}{(b^2-c^2)(b^2-a^2)}, \qquad (3a,b,c)$$

$$Z^2 = \frac{(c^2+\xi)(c^2+\eta)(c^2+\zeta)}{(c^2-a^2)(c^2-b^2)}.$$

Since a set of values of (ξ, η, ζ) determine eight points in the X, Y, Z-space, these relations are not unique.

2.2 Ellipsoidal Transformation

A unique transformation may be achieved by introducing the angular variables ψ and θ[14], so that

$$X = \sqrt{\xi+a^2}\ \cos\psi, \qquad 0 \leq \psi \leq \pi,$$

$$Y = \sqrt{\xi+b^2}\ \sin\psi\cos\theta, \qquad 0 \leq \theta \leq 2\pi, \qquad (4a,b,c)$$

$$Z = \sqrt{\xi+c^2}\ \sin\psi\sin\theta.$$

Since the relations between (ψ,θ) and (η,ζ) can be readily found from Eqs. (3b,c) and (4b,c), the details are not given here. On the ellipsoid $(\xi = 0)$, Eqs. (4a,b,c) become

$$X = a \cos \psi ,$$

$$Y = b \sin \psi \cos \theta , \qquad (5a,b,c)$$

$$Z = c \sin \psi \sin \theta .$$

This transformation yields a unique correspondence between (X,Y,Z) and (ξ,ψ,θ), resembling the more familiar spherical coordinates. However, the surfaces with ξ, θ, ψ, respectively, constants, are not orthagonal to one another; hence (ξ, θ, ψ) do not form an orthagonal coordinate system which can be used, for example, to replace the system (ξ, η, ζ) for obtaining the inviscid solution. The purpose here is simply to incorporate later the coordinates (ψ,θ) in order to form a boundary layer coordinate system which does not require orthagonality except on the body surface.

Geometrically, for an arbitrary point Q on the ellipsoid, the correspondence between (X,Y,Z) and (ξ, θ, ψ) is illustrated in Figs. 3a,b. It must be emphasized that both θ and ψ are eccentric angles. Fig. 3a shows how X_Q is related to ψ. Substituting $X_Q = a \cos \psi$ into Eq. (1) indicates that the cross section at $X = X_Q$ is an ellipse given by

$$\frac{Y^2}{b^2 \sin^2 \psi} + \frac{Z^2}{c^2 \sin^2 \psi} = 1.$$

Fig. 3b shows how, in this cross section, the coordinates Y_Q and Z_Q are related to θ. Fig. 3(c) shows the coordinate nets on the ellipsoid surface, consisting of the θ-constant lines and the x- or ψ- constant lines. These two sets of coordinate lines are orthagonal to each other.

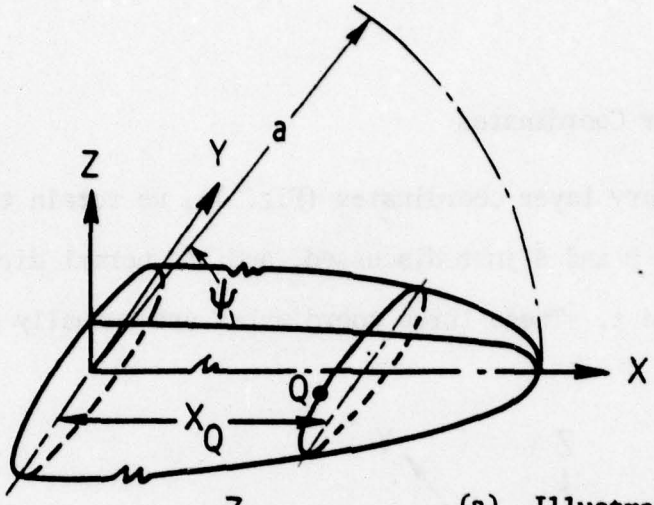

(a) Illustrating X_Q with ψ

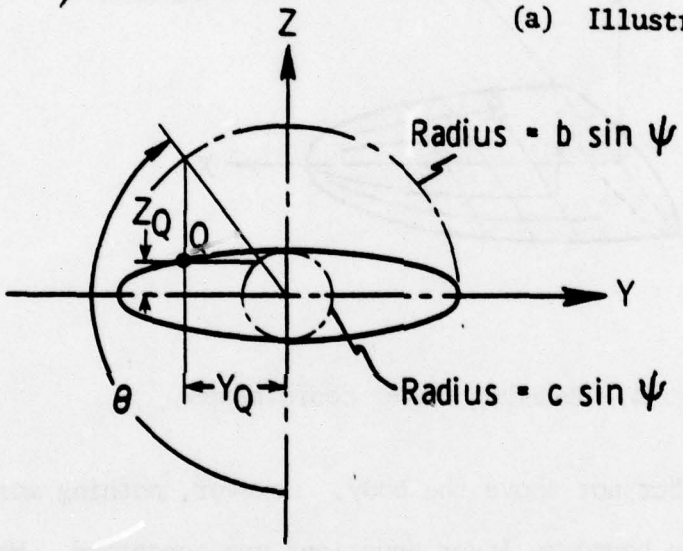

(b) Illustrating (Y_Q, Z_Q) with (ψ,θ)

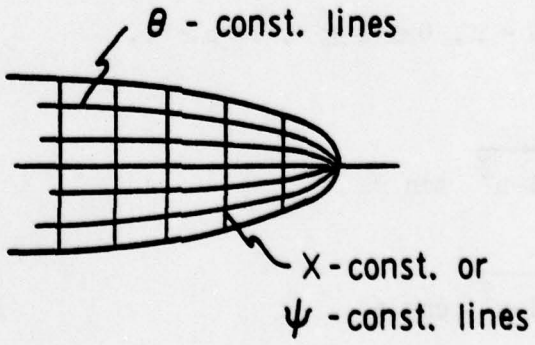

(c) Surface coordinate nets

Fig. 3. Geometric correspondence between (X,Y,Z) and (ξ,θ,ψ)

2.3 Boundary Layer Coordinates

For the boundary layer coordinates (Fig. 4), we retain the two surface coordinates ψ and θ just discussed, and the normal direction to the body, designated z. These three coordinates are mutually orthogonal

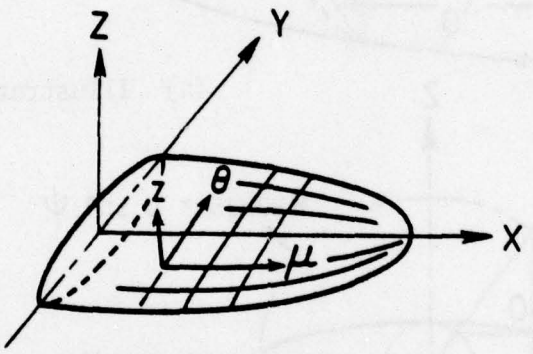

Fig. 4. Boundary layer coordinates

on the body surface, but not above the body. However, nothing more is required as far as the boundary layer equations are concerned. We shall further introduce μ to replace ψ so that,

$$\frac{X}{a} = \cos\psi = \mu, \quad 0 \leq \psi \leq \pi, \quad 1 \geq \mu \geq -1,$$

and

$$\frac{Y}{a} = \frac{-b}{a}\sqrt{1-\mu^2}\ \sin\theta \qquad (6a,b,c)$$

$$\frac{Z}{a} = \frac{-c}{a}\sqrt{1-\mu^2}\ \cos\theta$$

The (μ,θ,z) system is very similar to that used in our previous investigations for the body problem except that θ here is an eccentric angle. As a measure of length along the X-direction, μ is more convenient than ψ. One can, of course, also introduce $\nu = \cos\theta$ in analogy to $\mu = \cos\psi$, so that

$$X/a = \cos\phi = \mu,$$

$$Y/a = \frac{b}{a}\sqrt{1-\mu^2}\sqrt{1-\nu^2}, \qquad (7a,b,c)$$

$$Z/a = \frac{c}{a}\sqrt{1-\mu^2}\,\nu\,.$$

However, in using ν one must take care of the positive and negative signs for Y and Z in the range $0 \leq \theta \leq 2\pi$.

3. INVISCID FLOW INPUTS

3.1 Velocity Potential

Consider all the length coordinates, cartesian or curvilinear, to be non-dimensionalized by a, the major semi-axis, and retain the same symbols, X, Y, Z and ξ, μ, ζ for the dimensionless variables. The velocity potential ϕ is non-dimensionalized by V_∞ a, velocities by V_∞ and pressure by ρV_∞^2.

The potential ϕ, due to a uniform flow (non-dimensionalized) cos α along the Y-direction past an ellipsoid (Fig. 1) is given by[6]

$$\phi_1 = Y \cos\alpha + \frac{r_1 r_2}{2-\beta_0} (\cos\alpha) Y \int_\xi^\infty \frac{d\xi}{(\xi+r_1^2)\delta} , \qquad (8a)$$

where

$$r_1 = b/a, \quad r_2 = c/a,$$

$$\delta = \left[(\xi+1)(\xi+r_1^2)(\xi+r_2^2)\right]^{1/2} , \qquad (8b,c,d)$$

and

$$\beta_0 = r_1 r_2 \int_o^\infty \frac{d\xi}{(\xi+r_1^2)\delta} .$$

On the surface, $\xi = 0$, the potential becomes,

$$\phi_{1s} = \frac{2 \cos\alpha}{2 - \beta_0} Y_s , \qquad (8e)$$

where the subscript s denotes the body's surface.

Similarly for a uniform flow sin α past an ellipsoid along the Z-direction, the corresponding potential is

$$\phi_2 = Z \sin\alpha + \frac{r_1 r_2}{2-\gamma_0} (\sin\alpha)\, Z \int_\xi^\infty \frac{d\xi}{(\xi+r_2^2)\delta} , \tag{9a}$$

where

$$\gamma_0 = r_1 r_2 \int_o^\infty \frac{d\xi}{(\xi+r_2^2)\delta} . \tag{9b}$$

On the body,

$$\phi_{2s} = \frac{2 \sin\alpha}{2-\gamma_0} Z_s . \tag{9c}$$

Thus, for an ellipsoidal wing at incidence as depicted in Fig. 1, the resulting potential is obtained by superimposition,

$$\phi = \phi_1 + \phi_2 ,$$

and (10a, b)

$$\phi_s = \phi_{1s} + \phi_{2s} .$$

The method of evaluating the elliptical integrals is given in the Appendix.

3.2 Surface Flow in Terms of (μ,θ)

For later boundary layer study, the inviscid solutions must be expressed in terms of the surface coordinates (μ, θ). To do this we first rewrite Eqs. (6a,b,c) in non-dimensional form.

$$X = \mu,$$

$$Y = -r_1 \sqrt{1-\mu^2} \sin\theta,$$

$$Z = -r_2 \sqrt{1-\mu^2} \cos\theta,$$

from which the metric coefficients h_μ and h_θ are found to be

$$h_\mu = \left[\left(\frac{\partial X}{\partial \mu}\right)^2 + \left(\frac{\partial Y}{\partial \mu}\right)^2 + \left(\frac{\partial Z}{\partial \mu}\right)^2\right]^{1/2}$$

$$= \left[\frac{1-\mu^2(1-r_1^2 \sin^2\theta - r_2^2\cos^2\theta)}{1-\mu^2}\right]^{1/2} \qquad (11a)$$

$$h_\theta = \left[\left(\frac{\partial X}{\partial \theta}\right)^2 + \left(\frac{\partial Y}{\partial \theta}\right)^2 + \left(\frac{\partial Z}{\partial \theta}\right)^2\right]^{1/2}$$

$$= (1-\mu^2)^{1/2}\left[r_1^2\cos^2\theta + r_2^2 \sin^2\theta\right]^{1/2}. \qquad (11b)$$

We denote the surface velocities along the μ, θ-coordinates by U and V so that

$$U = \frac{\partial \phi_s}{h_\mu \partial \theta}, \qquad (12a,b)$$

$$V = \frac{\partial \phi_s}{h_\theta \partial \theta}.$$

Substituting in

$$U = \frac{1}{h_\mu} \frac{\mu}{\sqrt{1-\mu^2}} \left(g_1 \sin\theta + g_2 \cos\theta\right),$$

$$V = \frac{1}{h_\theta} \sqrt{1-\mu^2} \left(-g_1\cos\theta + g_2 \sin\theta\right), \qquad (12c,d)$$

$$= \frac{-g_1\cos\theta + g_2 \sin\theta}{\left(r_1^2 \cos^2\theta + r_2^2\sin^2\theta\right)^{1/2}},$$

where

$$g_1 = \frac{2\cos\alpha}{2-\beta_0} r_1 , \qquad (12e,f)$$

$$g_2 = \frac{2\sin\alpha}{2-\gamma_0} r_2 .$$

It is noteworthy that V is independent of μ.

The surface pressure is given by

$$p - p_\infty = \frac{1}{2}\left[1 - (U^2+V^2)\right]. \qquad (13)$$

With some manipulations, one finds the pressure gradients

$$\frac{\partial p}{h_\mu \partial\mu} = -\frac{1}{h_\mu} \frac{U^2}{\mu\left[1-\mu^2(1-r_1^2\sin^2\theta-r_2^2\cos^2\theta)\right]} , \qquad (14a)$$

$$\frac{\partial p}{h_\theta \partial\theta} = -\frac{U}{h_\theta} \frac{\mu(g_1\cos\theta-g_2\sin\theta)}{\left[1-\mu^2(1-r_1^2\sin^2\theta-r_2^2\cos^2\theta)\right]^{1/2}}$$

$$-\frac{U^2}{h_\theta} \frac{(-r_1^2+r_2^2)\mu^2\sin\theta\cos\theta}{1-\mu^2\left(1-r_1^2\sin^2\theta-r_2^2\cos^2\theta\right)}$$

$$-\frac{V}{h_\theta} \frac{g_1\sin_\theta+g_2\cos_\theta}{\left(r_1^2\cos^2\theta+r_2^2\sin^2\theta\right)^{1/2}}$$

$$-\frac{V^2}{h_\theta} \frac{(r_1^2-r_2^2)\sin\theta\cos\theta}{(r_1^2\cos^2\theta+r_2^2\sin^2\theta)} . \qquad (14b)$$

3.3 Pressure Distribution

Sample pressure distribution for an ellipsoid with a : b : c = 30 :6 : 1 at $\alpha = 10°$ is shown in Fig. 5. Although for a wing-like geometry the gradients around the leading edge and the tip are usually very large, they are finite. This highlights the importance of avoiding the linearized thin-wing theory in the present work. The linearized theory always yields a singular solution at the edges, which, in turn, prevents the boundary layer there from being determined. Consequently, the boundary layers on the upper and lower surfaces must be treated separately as if they were independent, and there is no single complete boundary layer solution on a finite wing at incidence.

A recent paper by Bluford[15] reports a Navier-Stokes solution over a delta wing. It should not be assumed that once a Navier-Stokes solution is obtainable, the simpler boundary layer problem (for a finite wing) will automatically become easy. In this regard it should be pointed out that the Navier-Stokes solution was obtained with additional constraints, among which are the assumption of the conical flow and of the independence between the flows above and below the wing surface. This is not intended as a criticism of this outstanding paper, but merely to point out the current state of knowledge of viscous flow over a finite wing.

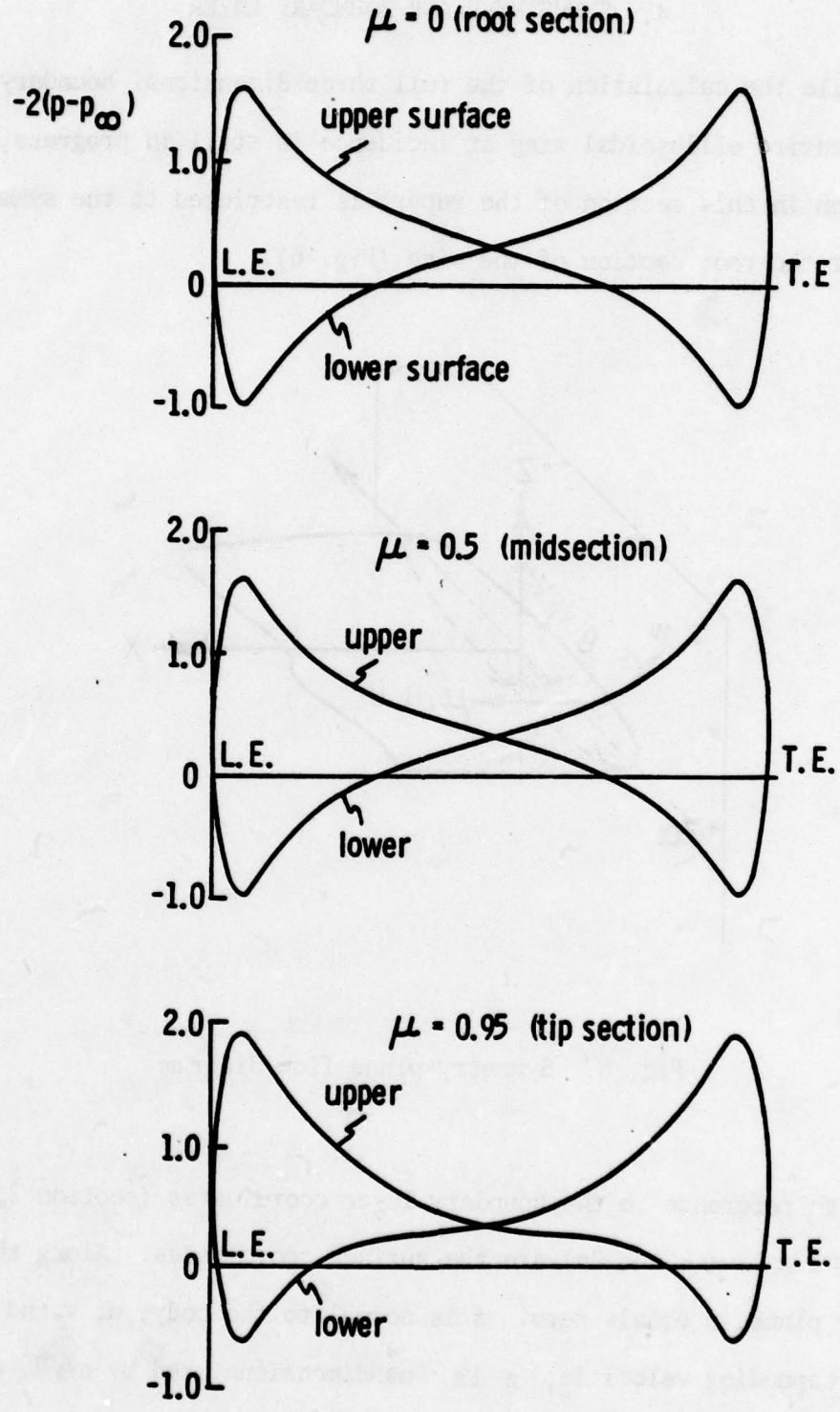

Fig. 5. Surface pressure distribution at chordwise sections

4. SYMMETRY-PLANE BOUNDARY LAYER

While the calculation of the full three-dimensional boundary layer over an entire ellipsoidal wing at incidence is still in progress, consideration in this section of the report is restricted to the symmetry-plane, or the root section of the wing (Fig. 6).

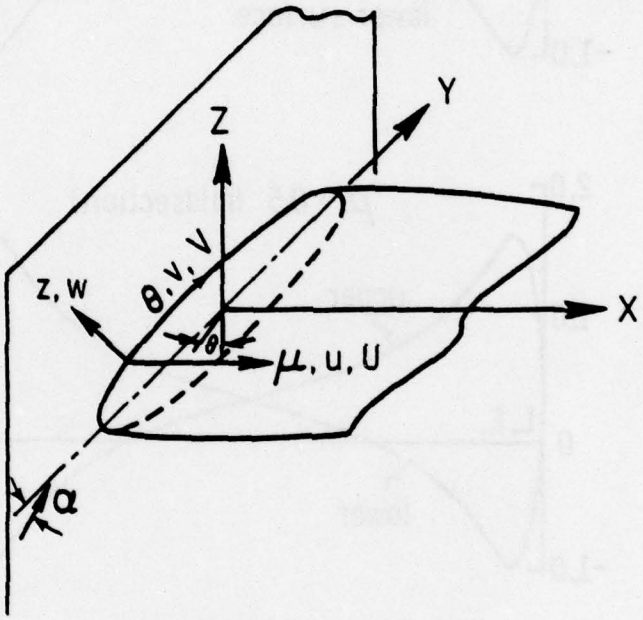

Fig. 6. Symmetry-plane flow diagram

With reference to the boundary layer coordinates (section 2), μ and θ ($-1 < \mu \leq 1$, $0 \leq \theta \leq 2\pi$) are the surface coordinates. Along the symmetry plane, μ equals zero. z is normal to the body; u, v and w are the corresponding velocitie, z is nondimensionalized by $a/\sqrt{R}$, where $R(=Va/\nu^*$, ν^* the kinematic viscosity) is the Reynolds number, w by $V_\infty/\sqrt{R}$.

u, v are non-dimensionalized with V_∞, other inviscid variables such as U, V, p were already defined in Section 4.

Along the symmetry-plane,

$$u \equiv \frac{\partial u}{\partial \theta} \equiv \frac{\partial u}{\partial z} \equiv \frac{\partial^2 u}{\partial z^2} \equiv U \equiv \frac{\partial U}{\partial \theta} \equiv 0, \tag{15a,b}$$

$$\frac{\partial v}{\partial \mu} = \frac{\partial w}{\partial \mu} = \frac{\partial p}{\partial \mu} = 0.$$

From Eqs. (11a, b), we also have with $\mu = 0$,

$$h_\mu = 1,$$

$$h_\theta = \left(r_1^2 \cos^2\theta + r_2^2 \sin^2\theta\right)^{1/2}, \tag{16a,b}$$

$$\frac{\partial h_\theta}{\partial \mu} = \frac{\partial h_\mu}{\partial \theta} = \frac{\partial h_\mu}{\partial \mu} = 0.$$

4.1 Boundary Layer Equations

In virtue of Eqs. (15a,b and 16a,b) the pertinent symmetry-plane boundary layer equations become,

$$\frac{\partial v}{h_\theta \partial \theta} + \frac{u_\mu}{h_\mu} + \frac{\partial w}{\partial z} = 0,$$

$$\frac{v \partial v}{h_\theta \partial \theta} + w \frac{\partial v}{\partial z} = \frac{-\partial p}{h_\theta \partial \theta} + \frac{\partial^2 v}{\partial z^2}, \tag{17a,b,c}$$

$$\frac{v \partial u_\mu}{h_\theta \partial \theta} + w \frac{\partial u_\mu}{\partial z} + \frac{(u_\mu)^2}{h_\mu} - \frac{v^2}{h_\mu h_\theta} \frac{\partial}{\partial \mu}\left(\frac{\partial h_\theta}{\partial \mu}\right)$$

$$= -\frac{\partial}{\partial \mu}\left(\frac{\partial p}{h_\mu \partial \mu}\right) + \frac{\partial^2 u_\mu}{\partial z^2}.$$

Along with v and w, $u_\mu (= \partial u/\partial\mu)$ is treated here as an unknown entity by three equations in two coordinate variables, θ and z, subject to the boundary conditions,

$$v = V, \quad u_\mu = U_\mu \left(= \frac{\partial U}{\partial \mu}\right) \quad \text{at } z \to \infty,$$
$$v = w = u_\mu = 0 \qquad \text{at } z = 0. \tag{18a,b}$$

As V is independent of μ, it remains the same as given in Eq. 12d. With $\mu = 0$, other inviscid inputs become

$$U_\mu = \frac{\partial U}{\partial \mu} = g_1 \sin\theta + g_2 \cos\theta,$$

$$\frac{\partial p}{h_\theta \partial\theta} = \frac{-V(g_1 \sin\theta + g_2 \cos\theta)}{h_\theta \left(r_1^2 \cos^2\theta + r_2^2 \sin^2\theta\right)^{1/2}}$$

$$-\frac{V^2}{h_\theta} \frac{(r_1^2 - r_2^2)\cos\theta \sin\theta}{(r_1^2 \cos^2\theta + r_2^2 \sin^2\theta)}, \tag{19a,b,c,d}$$

$$\frac{\partial}{\partial\mu}\left(\frac{\partial p}{h_\mu \partial\mu}\right) = \frac{\partial^2 p}{h_\mu \partial\mu^2} = -U_\mu^2,$$

$$\frac{\partial}{\partial\mu}\left(\frac{\partial h_\theta}{\partial\mu}\right) = -\left(r_1^2 \cos^2\theta + r_2^2 \sin^2\theta\right)^{1/2} = -h_\theta.$$

The skin friction $c_{f\theta}$ is defined by

$$c_{f\theta} = \frac{1}{\sqrt{R}} \left(\frac{\partial v}{\partial z}\right) z \to 0, \tag{20}$$

and the replacement thickness Δ_θ is likewise defined by

$$\Delta_\theta = \int_0^\infty (1-v/V)dz. \tag{21}$$

4.2 Method of Solution

The same methods and computing programs were employed for the solution as those previously used for the symmetry-plane boundary layer over an inclined body of revolution. The stagnation-point boundary layer was solved first using a separate computing program previously developed in accordance with the Howarth-Squire solution[16]. Then the existing symmetry-plane boundary layer program was modified for the present application. On the lower surface, computation began at the stagnation-point, marching straight toward the separation point. For the upper surface, computation must first pass through the leading-edge, continuing toward the trailing edge.

The coordinate θ is very convenient for uniquely designating points at different quadrants on the lower and upper surfaces, but such an eccentric angle does not indicate directly the corresponging location on the wing. As a minor variation to Eqs. (7a,b,c), we introduce a chordwise coordinate

$$\nu = \cos\ (270^\circ - \theta),\ 0 \leqq \theta \leqq 2\pi,\ -1.0 \leqq \nu \leqq 1.0,$$

so that in following the usual convention, ν equals +1.0 at the trailing edge ($\theta = 270^\circ$) and -1.0 at the leading edge ($\theta = 90^\circ$) as shown in Fig. 7. The distinction between the upper and lower surfaces will be explicitly stated.

We shall use θ during the calculations, and use ν along with θ in presenting the results.

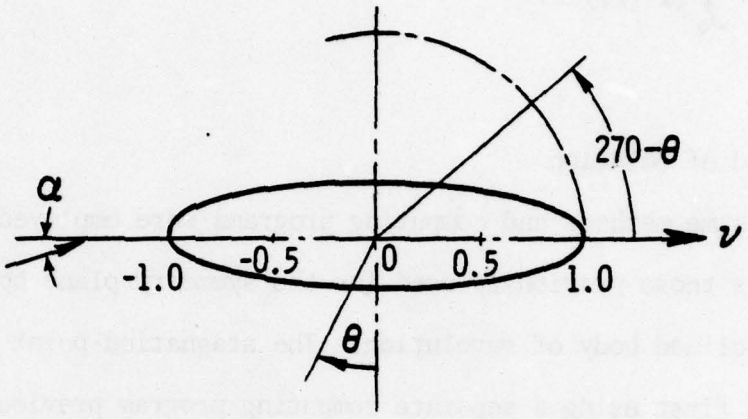

Fig. 7. Coordinate ν

4.3 Results

To identify the separation jump phenomenon and to establish some basic trends, calculations were made for four different cases, corresponding to four different axis-ratios a:b:c, each at various incidences.

4.3.1 Case 1 - Typical Problem

Calculation for the first case was based upon axis-ratios a:b:c equal to 30:6:1. This corresponds to a typical situation for the conventional, large aspect-ratio wing. Fig. 8 shows the pressure distribution on the upper surface. Characteristically, negative pressure prevails near the leading edge. As the incidence increases, the pressure gradient becomes larger. The lower-surface pressure distribution is symmetric to the upper-surface pressure distribution about the center line (Fig. 8), so that negative

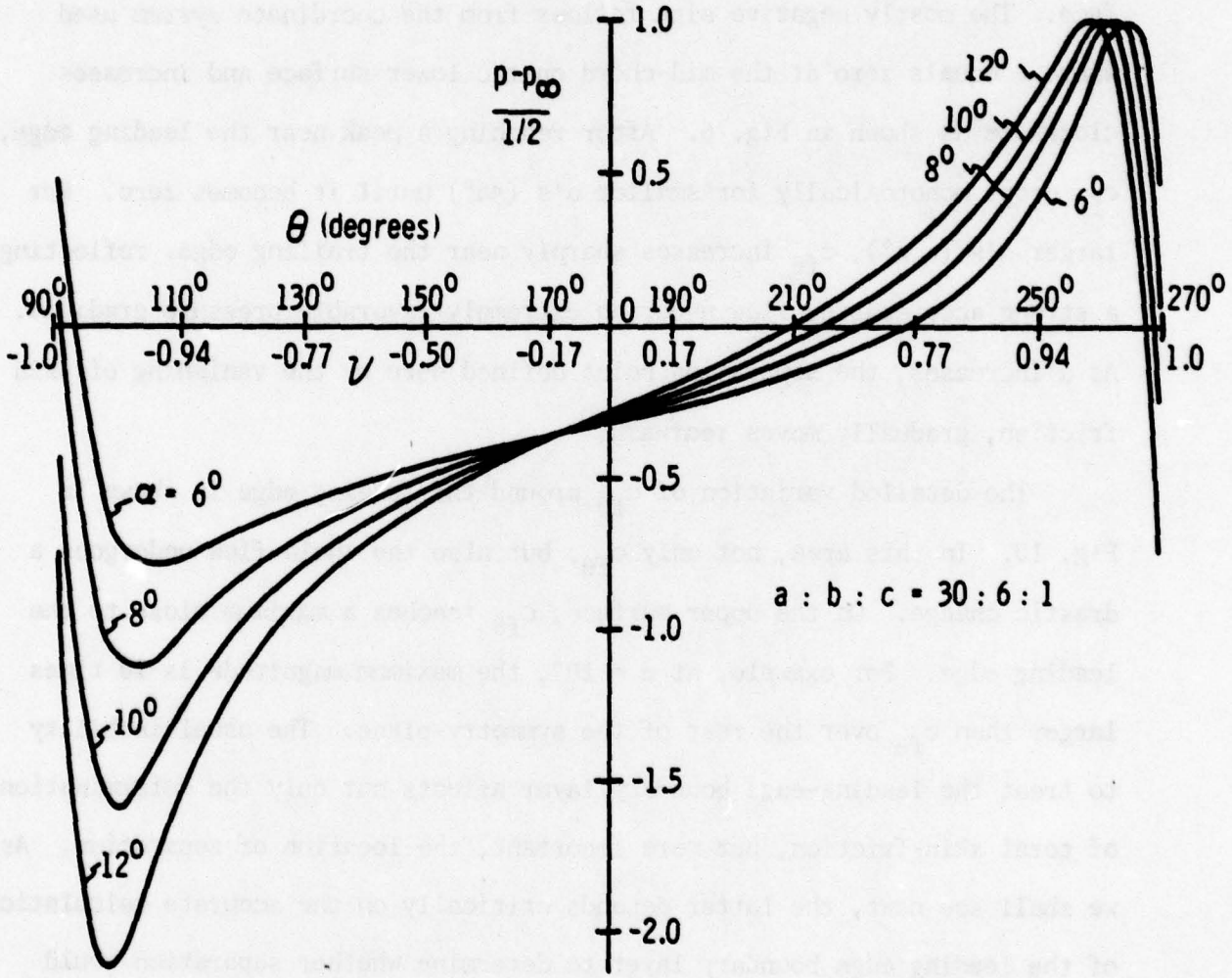

Fig. 8. Pressure distribution on the upper surface

pressure would prevail near the trailing edge instead of the leading edge. Note that along the abscissa both scales of θ and ν are shown.

Fig. 9 shows the skin-friction ($c_{f\theta}$) distribution on the lower surface. The mostly negative sign follows from the coordinate system used where θ equals zero at the mid-chord on the lower surface and increases clockwise as shown in Fig. 6. After reaching a peak near the leading edge, $c_{f\theta}$ drops monotonically for smaller α's ($<6°$) until it becomes zero. For larger α's ($> 6°$), $c_{f\theta}$ increases sharply near the trailing edge. reflecting a strong accelerating flow under an extremely favorable pressure gradient. As α increases, the separation point defined here by the vanishing of skin friction, gradually moves rearward.

The detailed variation of $c_{f\theta}$ *around the leading-edge is shown in* Fig. 10. In this area, not only $c_{f\theta}$, but also the whole flow undergoes a drastic change. On the upper surface, $c_{f\theta}$ reaches a maximum close to the leading edge. For example, at $\alpha = 10°$, the maximum magnitude is 10 times larger than $c_{f\theta}$ over the rest of the symmetry-plane. The usual inability to treat the leading-edge boundary layer affects not only the determination of total skin-friction, but more important, the location of separation. As we shall see next, the latter depends critically on the accurate calculation of the leading-edge boundary layer to determine whether separation would take place near the leading-edge or further downstream.

The skin friction behavior on the upper surface is more interesting (Fig. 11). When the incidence remains below 10.5°, $c_{f\theta}$ always drops monitonically until it becomes zero, and the separation point moves continually forward. At $\alpha = 10.75°$, the skin friction decreases first to a minimum and

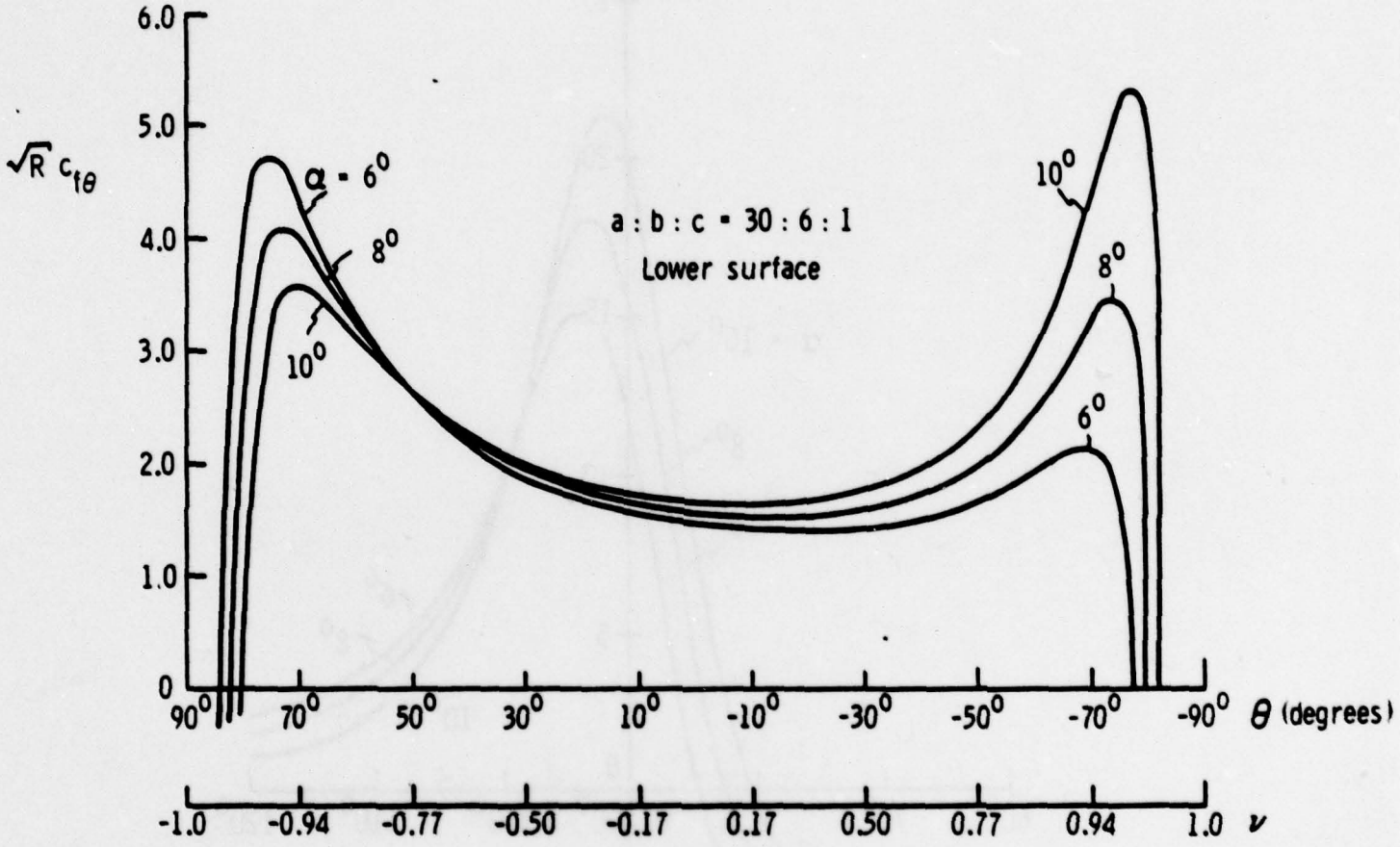

Fig. 9. Skin friction on the lower surface

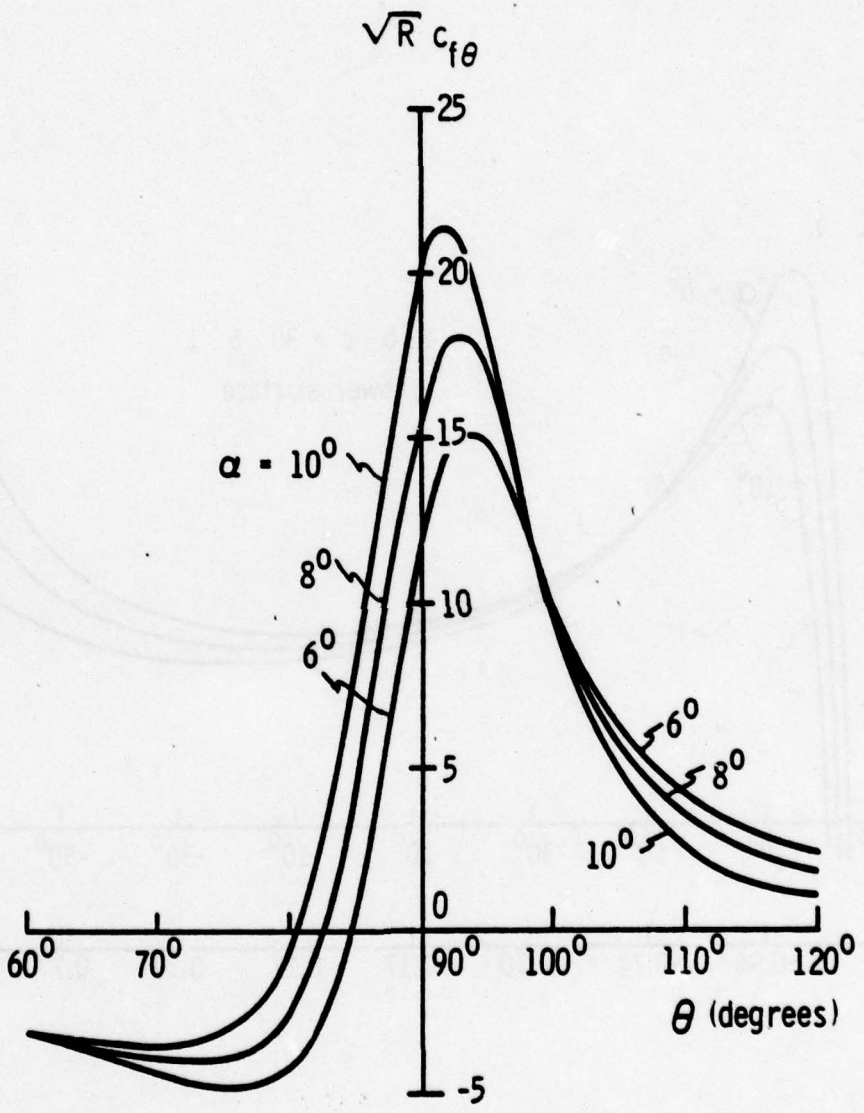

Fig. 10. Skin friction around the leading edge

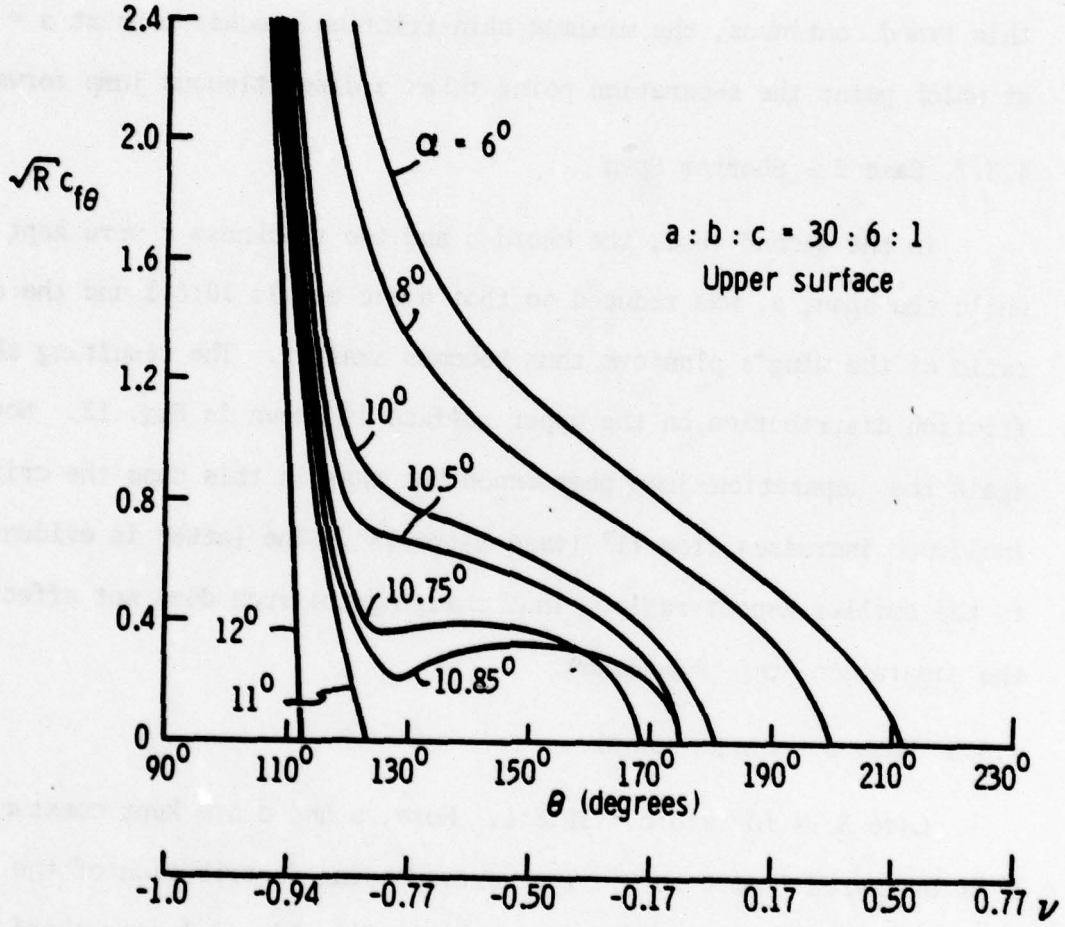

Fig. 11. Skin friction on the upper surface

then rises somewhat before finally falling to zero. At slightly higher incidence, $\alpha = 10.85°$, the minimum skin-friction point further shifts downward, and the separation point moves rearward instead of forward. As this trend continues, the minimum skin-friction touches zero at $\alpha = 11°$, at which point the separation point takes a discontinuous jump forward.

4.3.2 Case 2 - Shorter Span

In the second case, the chord b and the thickness c were kept fixed, while the span, a, was reduced so that a:b:c equals 10:6:1 and the aspect-ratio of the wing's planform thus becomes smaller. The resulting skin-friction distribution on the upper surface is shown in Fig. 12. Notice again the separation-jump phenomenon but that in this case the critical incidence increases from 11° (case 1) to 13°. The latter is evidently due to the smaller aspect-ratio. Thus changing the span does not affect much the separation-jump phenomenon.

4.3.3 Case 3 - Longer Chord

Case 3 is for a:b:c = 30:8:1. Here, a and c are kept constant, while b is increased from 6 to 8. The corresponding distribution of the skin friction on the upper surface is shown in Fig. 13. A longer chord makes the wing more sensitive to an increase of incidence. The non-monotonic decrease of skin friction as a characteristic of the separation jump phenonemom becomes noticeable at smaller incidence, and the critical incidence for the jump decreases to $\alpha = 8.7°$. Of the first three cases studied, the jump for case 3 is the most pronounced and covers more than half of the chord length. Hence, an increase of b with a and c fixed considerably enhances the "separation jump" phenomenon.

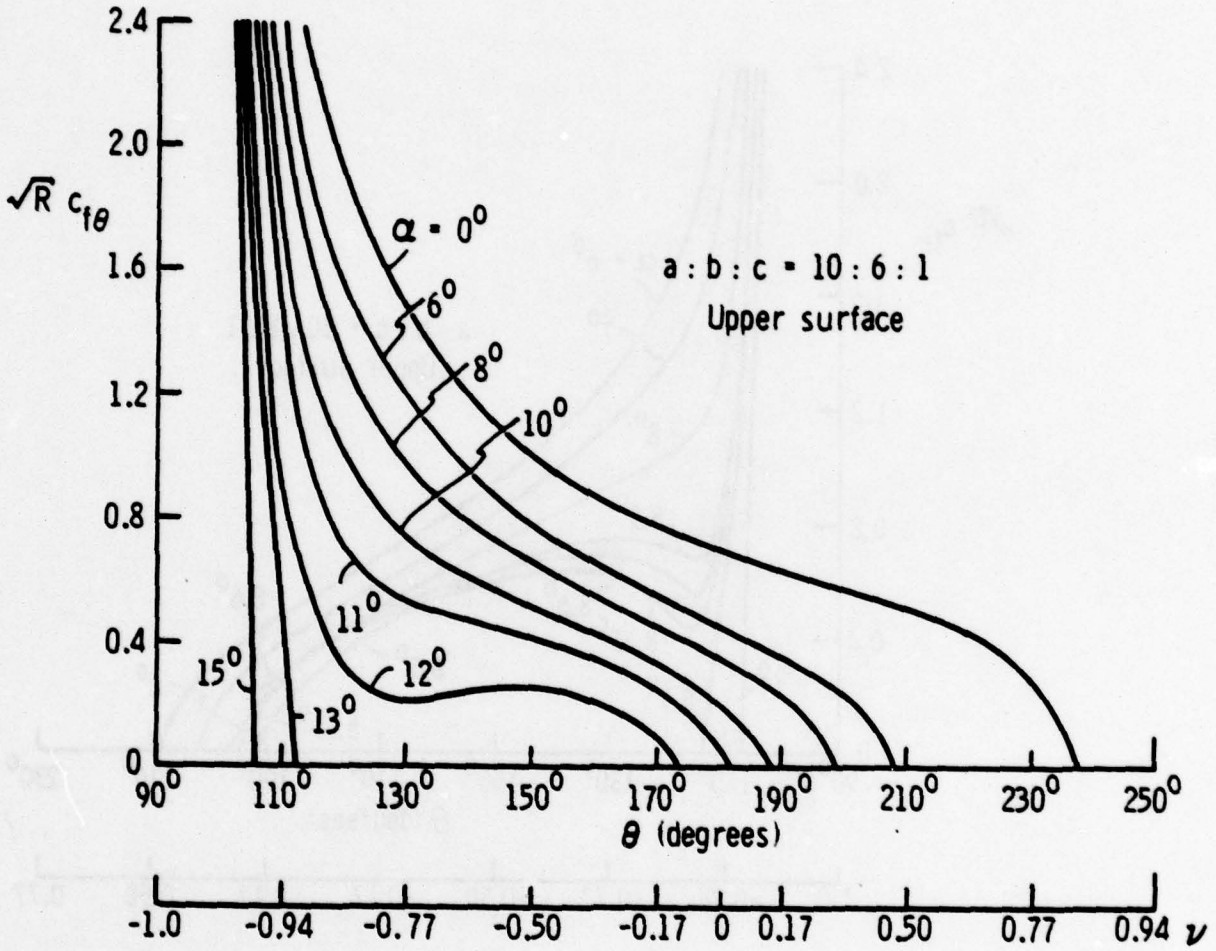

Fig. 12. Skin friction on the upper surface

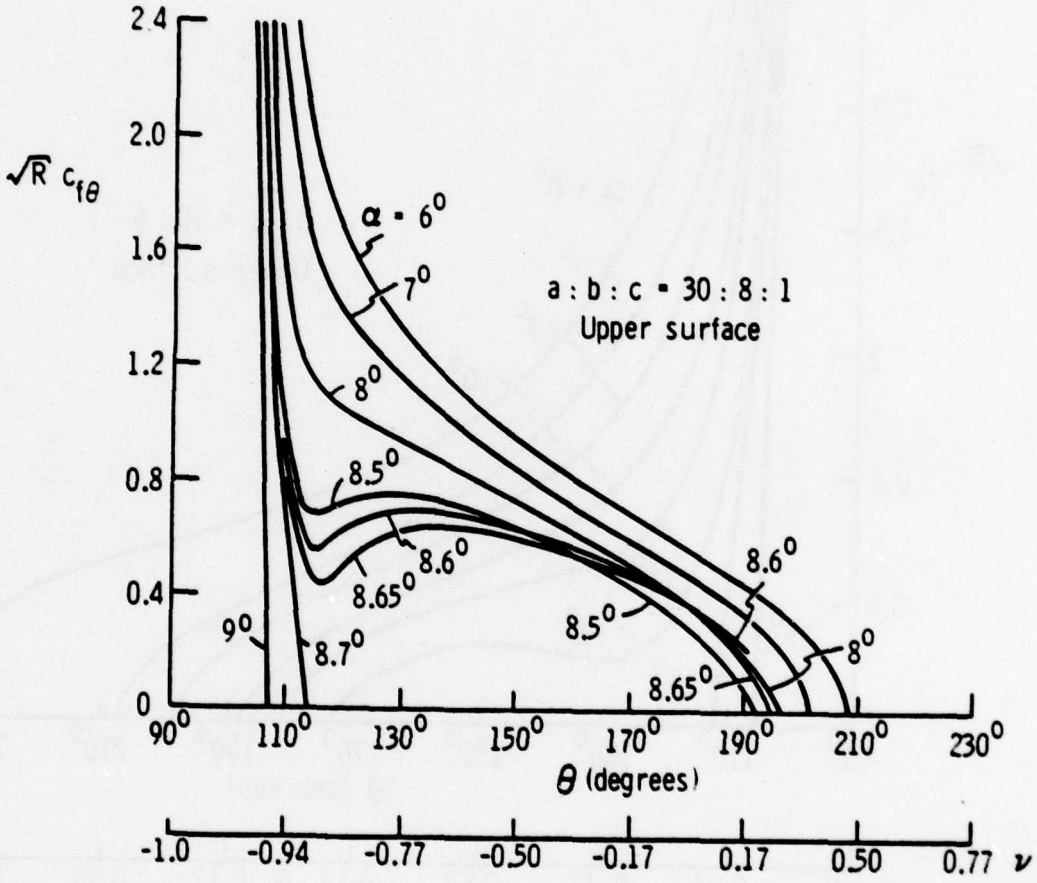

Fig. 13. Skin friction on the upper surface

4.3.4 Case 4 - Shorter Chord

Case 4 is for a:b:c = 20:5:1. In comparison with case 1, the span a is reduced from 30 to 20 and the chord b is reduced from 6 to 5. The resulting upper-surface skin friction $c_{f\theta}$ is shown in Fig. 14. Surprisingly, for all incidences, $c_{f\theta}$ always decreases monotonically to zero; the separation point moves forward continuously; and the afore-noted separation jump was not found. In case 2, we noted that reduction of a from 30 to 10 with b and c held constant does not affect the separation jump; hence, the disappearance of the separation jump for the present case 4 must be due to the shortening of b rather than a. In other words, a shorter chord tends to reduce or even to eliminate the separation jump. This conclusion agrees with the conclusion from case 3; i.e., the separation jump depends critically on the chord/thickness ratio, with a longer chord tending to prompt a larger jump.

4.3.5 Separation Versus Incidence

The location of the separation point with respect to the incidence for the four cases considered is summarized in Fig. 15. The curves are numbered according to the cases studied. In case 1, as α increases from 6°, the separation point moves gradually forward, at $\alpha = 10.85°$ it begins to move rearward; and at $\alpha = 11°$, it jumps to near the leading edge. The jump for case 3 is the most drastic whereas case 4 shows no jump at all. It is understood that for $\alpha < 6°$, the separation point always moves forward with increasing incidence. Results for such low incidences have not been included in this report because they are not relevant to the main theme of separation jump.

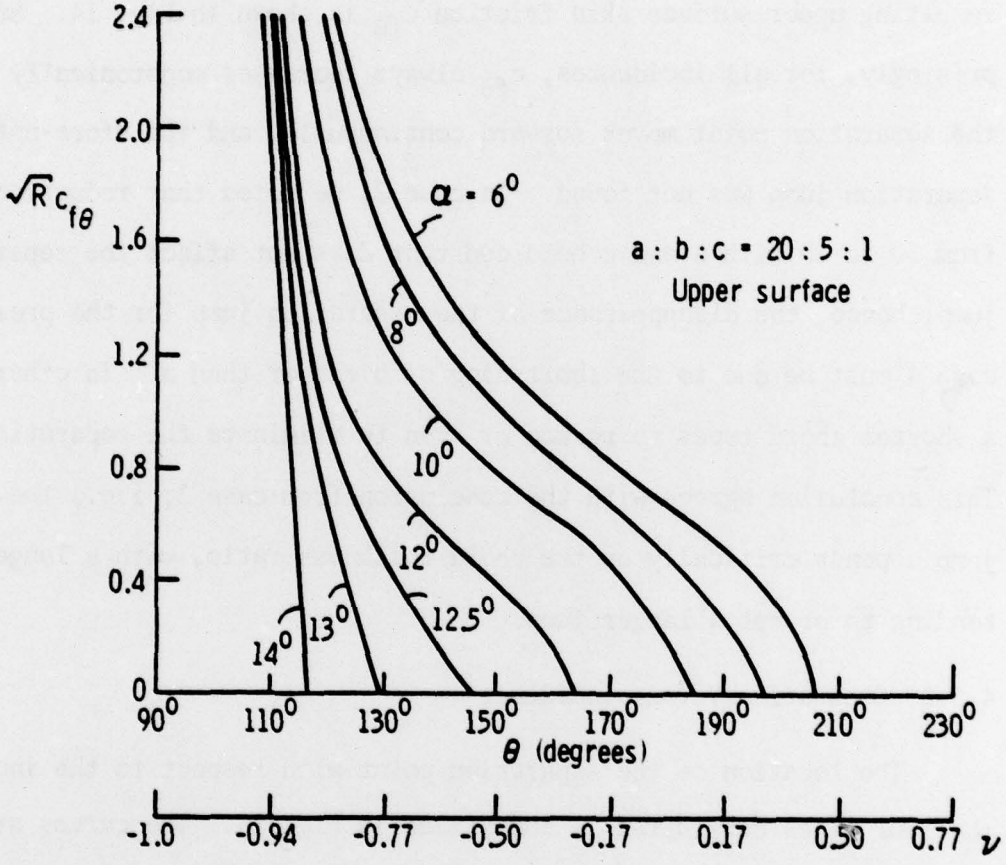

Fig. 14. Skin friction on the upper surface

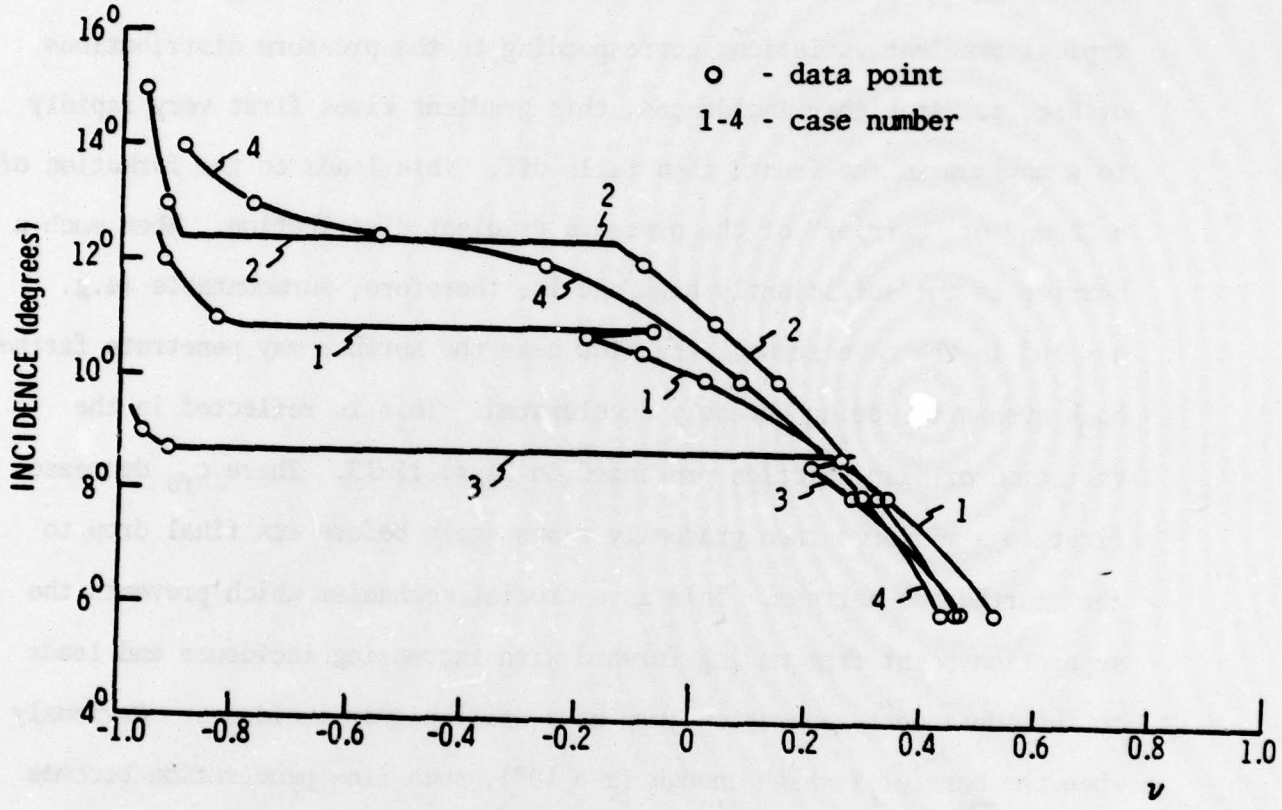

Fig. 15. Movement of the upper-surface separation point versus incidence

4.3.6 Jump Mechanism

The reason for the occurrence of separation jump with a flat wing is as was the case for an inclined body of revolution[9,10], i.e., the barrier of the pressure gradient over the front chord. Fig. 16 shows typical gradient variations corresponding to the pressure distributions of Fig. 8. At higher incidences, this gradient rises first very rapidly to a maximum in the front, then falls off. This leads to the formation of a "hump" or "barrier" of the pressure gradient distribution. When such a barrier is not sufficiently high and is, therefore, surmountable (e.g. $\alpha < 10°$ in the case shown), the flow near the surface may penetrate farther back even after being severely decelerated. This is reflected in the variation of skin friction presented in Figs. 11-13. There $c_{f\theta}$ decreases first to a minimum, then gradually rises again before its final drop to zero further downstream. This is a crucial mechanism which prevents the separation point from moving forward with increasing incidence and leads to the subsequent separation jump at a still higher incidence. Obviously when the barrier is high enough ($\alpha > 10°$), such flow penetration becomes increasingly difficult. At some critical incidence, the near-surface flow would be stopped near the leading edge and separation occurs immediately.

4.3.7 Sudden Stall

Whenever a separation jump occurs and the separation begins so close to the leading edge that stall is likely to follow, especially for the inner span. Since such a stall occurs suddenly as the incidence increases, it is therefore appropriate to call it "sudden stall."

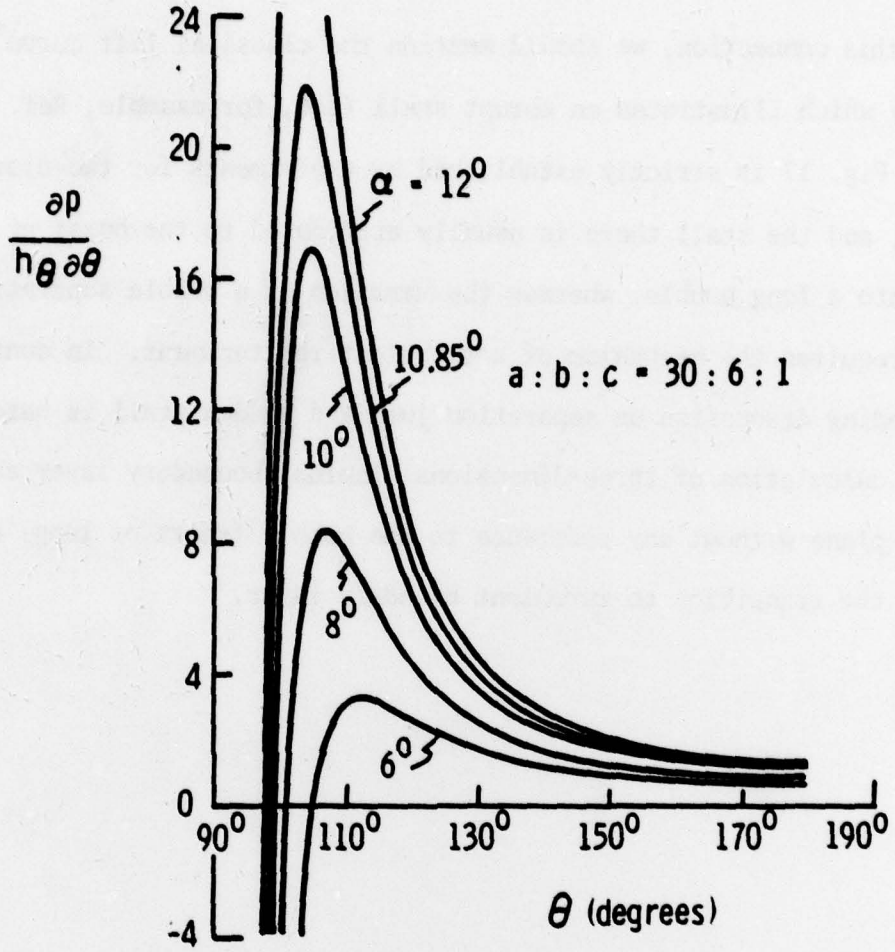

Fig. 16. Barrier of pressure gradient

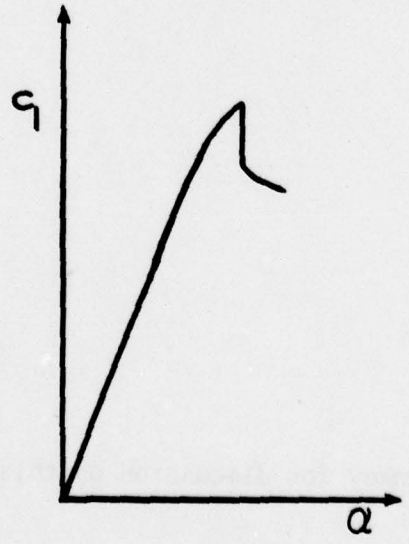

Fig. 17. Lift curve for an airfoil

In this connection, we should mention the classical lift curve* (Fig. 17) which illustrates an abrupt stall (see, for example, Ref. 18). However, Fig. 17 is strictly established by experiments for two-dimensional airfoils, and the stall there is usually attributed to the burst of a short bubble into a long bubble, whereas the formation of a bubble separation further requires the mechanism of a turbulent reattachment. In contrast, our preceding discussion on separation jump and sudden stall is based on straight calculation of three-dimensional laminar bounndary layer along the symmetry-plane without any reference to the bubble (short or long) separation and the transition to turbulent boundary layer.

---

*The author thanks Dr. W. Hankey for discussion on this question.

5. CONCLUSIONS

We have thus presented the results relating to the separation jump for a wing-like body. Although the literature on the wings flow is abundant, the separation jump phenomenon has never been reported before. It is especially noteworthy that the separation jump occurs at relatively high incidence within a narrow range of incidence. If systematic boundary layer calculations had not been carried out to sufficiently high incidence with small increments of incidence, the phenomenon could not have been discovered.

In previously reported studies involving an elongated body, once the separation on the windside and leeside symmetry-plane is systematically known for various incidences, a general separation pattern over the entire body can be readily visualized. Consequently, the separation jump phenomenon for the body problem led us immediately to propose the concept of open versus closed separation[11,12] long before the full three-dimensional boundary layer solutions[1,2] were obtained.

In the present wing study, the influence of the symmetry-plane flow is more restricted to the central portion of the wing. From our knowledge of the separation characteristics along the symmetry-plane, we have not been able to conceive a similar overall separation picture for an entire wing except that a sudden stall is likely to follow a separation jump, especially for the inner span.

Based on the symmetry-plane boundary-layer solutions, we conclude summarily:

1) The phenomenon of spearation jump on an inclined ellipsoidal wing has been determined.
2) Such a separation jump is not much affected by changes in span, but is greatly enhanced by a longer chord.
3) Separation jump is likely accompanied by a sudden stall.
4) Subject to further verification, real, finite wings are generally subject to separation jump and sudden stall.

6. REFERENCES

1. Wang, K. C., "Boundary Layer Over a Blunt Body at High Incidence with an Open-Type of Separation," Proc. Roy. Soc. London. Ser. A, 340, 33-55, 1974.

2. Wang, K. C., "Boundary Layer Over a Blunt Body at Low Incidence with Circumferential Reversed Flow," J. Fluid Mech. 72, 1, 49-65, 1975.

3. Sears, W. R., "The Boundary Layer of Yawed Cylinders," JAS, 15, 1, 49-52, 1948.

4. Jones, R. T., "Effects of Sweepback on Boundary Layer and Separation," NACA Rep. 884, 1947.

5. Prandtl, L., "On Boundary Layers in Three-Dimensional Flow," Rep. Aero. Res. Coun., London, No. 9828, 1946.

6. Lamb, H., Hydrodynamics. 6th Ed., Dover, 1945.

7. Eisenhart, L. P., Differential Geometry. Ginn & Co., 1909.

8. Zaat, J. A., E. Van Spiegel and Timman, R., "The Three-Dimensional Laminar Boundary Layer Flow about a Yawed Ellipsoid at Zero Incidence," Rep. F. 165 of The Nat. Aero. Res. Inst., 1952.

9. Wang, K. C., "Three-Dimensional Boundary Layer near the Plane of Symmetry of a Spheroid at Incidence," J. Fluid Mech., 43, 1, 187-209, 1970.

10. Laminar Boundary Layer near the Symmetry-Plane of a Prolate Spheroid," AIAA J., 12, 7, 949-958, 1974.

11. Wang, K. C., "Separation Patterns of Boundary Layer Over an Inclined Body of Revolution," AIAA J., 10, 8, 1044-1050, 1972.

12. Wang, K. C., "Separation of Three-Dimensional Flow," Proc. of the Lockheed-Georgia Company Viscous Flow Symposium, LG77ER0044, Atlanta, Ga., 341-414, 1977. Also Martin Marietta Labs TR 76-54c, 1976.

13. Cebeci, T., Khattab, A. K. and Stewartson, K., "Studies on Three-Dimensional Laminar and Turbulent Boundary Layer on Bodies of Revolution at Incidence. I. Noise Separation," AIAA Paper 79-0138, Jan. 1979.

14. Hobson, E. W., The Theory of Spherical and Ellipsoidal Harmonics. Chelsea Pub. Co., N. Y., 1955.

15. Bluford, G. S. Jr., "Numerical Solution of the Supersonic and Hypersonic Viscous Flow around Thin Delta Wings," AIAA Paper 78-1136, July 1978.

16. Squire, L. C., "The Three-Dimensional Boundary Layer Equations and Some Power Series Solutions," ARC Rep. and Mem. No. 3006, 1955.

17. Gröbner, W. and Hofreiter, N., Integraltafel, Erster Teil, pp. 78-79. Springer-Verlag, 1965.

18. Thwaites, B. Incompressible Aerodynamics. Oxford University Press, 1960.

APPENDIX

EVALUATION OF INTEGRALS

The method of evaluating the integral of the type

$$I = \int \frac{dx}{(x-\rho)\sqrt{(x-\alpha_1)(x-\alpha_2)(x-\alpha_3)}}, \quad \alpha_1 > \alpha_2 > \alpha_3 ,$$

can be found from integral tables[17]. The basic idea is to introduce a quadratic transformation

$$x = \frac{a \sin^2\phi + b}{c \sin^2\phi + d}, \quad 0 \leq \phi \leq \pi/2 ,$$

so that the integral can be expressed in terms of the Legendre's canonical forms of the elliptical integrals. In this Appendix, ϕ is just an angular variable (not a velocity potential as in section 3.1) following the conventional notation. For our problem, we let

$$a = -\alpha_2, \quad b = \alpha_1, \quad c = -1, \quad d = 1,$$

and write

$$\zeta = \alpha_1 - \alpha_2,$$

$$\sigma = (\alpha_1 - \alpha_2)\sqrt{\alpha_1 - \alpha_3} ,$$

$$k^2 = \frac{\alpha_2 - \alpha_3}{\alpha_1 - \alpha_3} ,$$

Substitution gives

$$I = \begin{cases} \frac{-2c}{\sigma}\left[\left(\delta + \frac{c}{k^2}\right) F(k,\phi) - \frac{c}{k^2} E(k,\phi)\right] + \text{const.}, \text{ for } \rho = \frac{a}{c}, \\ \\ \frac{2d}{\sigma}\left[(c+d)\, F(k,\phi) - dE(k,\phi) - d(c+g\phi)\sqrt{1-k^2\sin^2\phi}\right] + \text{const.}, \\ \qquad \text{for } \rho = \frac{b}{d}. \end{cases}$$

Where $F(\phi,k)$ and $E(\phi,k)$ are known as the elliptic integral of the first and the second kind,

$$F(k, \phi) = \int_0^{\phi} \frac{d\phi}{\sqrt{1-k^2\sin^2\phi}},$$

$$0 \leq k \leq 1$$

$$E(k, \phi) = \int_0^{\phi} \sqrt{1-k^2\sin^2\phi}\, d\phi.$$

The integral for β_0 corresponds to the case $\rho = \frac{a}{c}$, and that for γ_0 corresponds to $\rho = \frac{b}{d}$.

SECURITY CLASSIFICATION OF THIS PAGE (When Data Entered)

REPORT DOCUMENTATION PAGE		READ INSTRUCTIONS BEFORE COMPLETING FORM
1. REPORT NUMBER AFOSR-TR- 79-0965	2. GOVT ACCESSION NO.	3. RECIPIENT'S CATALOG NUMBER
4. TITLE (and Subtitle) SEPARATION JUMP AND SUDDEN STALL OVER AN ELLIPSOIDAL WING AT INCIDENCE		5. TYPE OF REPORT & PERIOD COVERED Interim 6. PERFORMING ORG. REPORT NUMBER
7. AUTHOR(s) K.C.Wang		8. CONTRACT OR GRANT NUMBER(s) F49620-76-C-0004
9. PERFORMING ORGANIZATION NAME AND ADDRESS Martin Marietta Laboratories 1450 South Rolling Road Baltimore, Maryland 21227		10. PROGRAM ELEMENT, PROJECT, TASK AREA & WORK UNIT NUMBERS 61102F 2304/A3
11. CONTROLLING OFFICE NAME AND ADDRESS Air Force Office of Scienctific Research/NM Bolling AFB, Washington, DC 20332		12. REPORT DATE May 1979 13. NUMBER OF PAGES 47
14. MONITORING AGENCY NAME & ADDRESS(if different from Controlling Office)		15. SECURITY CLASS. (of this report) UNCLASSIFIED 15a. DECLASSIFICATION/DOWNGRADING SCHEDULE

16. DISTRIBUTION STATEMENT (of this Report)

Approved for public release; distribution unlimited.

17. DISTRIBUTION STATEMENT (of the abstract entered in Block 20, if different from Report)

18. SUPPLEMENTARY NOTES

19. KEY WORDS (Continue on reverse side if necessary and identify by block number)

Numerical solutions; Wing theory; 3-D boundary layer; Flow separation; Aerodynamic stall

20. ABSTRACT (Continue on reverse side if necessary and identify by block number)

To obtain complete and rigorous solutions of the three-dimensional, laminar boundary layer over a finite airplane wing, a flat ellipsoid was chosen as a model to generate concrete results. Initial efforts were directed toward calculating the inviscid flow and the selection of coordinate system, and this was followed by a detailed investigation of the boundary layer restricted to the symmetry-plane. This investigation showed that as the incidence increases, the separation point on the upper surface does not always move continuously forward; instead, it first moves forward and later rearward.

DD 1 JAN 73 1473

UNCLASSIFIED

SECURITY CLASSIFICATION OF THIS PAGE (When Data Entered)

20. Abstract continued.

Then, at a critical incidence, it jumps forward and moves thereafter close to the leading edge. This "separation jump" phenomenon was further found to be little affected by varying the span, but critically dependent on the chord: a longer chord prompts a larger jump. Although such separation jump has been reported for a body of revolution, it has not yet been reported for wing surfaces. The significance of this pehnomenon is apparent when one considers that the separation jump may well occur on airplane wings in general and probably accounts for what we might call "sudden stall."